# RESEARCH PAPERS

*Acta Cryst.* (1997). B53, 189–202

## Effect of Habit Modification on Optical and X-ray Structures of Sodium Halate Mixed Crystals: The Etiology of Anomalous Double Refraction

GUY CRUNDWELL, PRAKASH GOPALAN, ALEX BAKULIN, MATTHEW L. PETERSON AND BART KAHR*

*Department of Chemistry, Purdue University, West Lafayette, IN 47907-1393, USA. E-mail: kahr@chem.purdue.edu*

(*Received 2 May 1996; accepted 2 August 1996*)

### Abstract

Structures of mixed crystals of the isomorphous salts $NaClO_3$ and $NaBrO_3$ (sodium chlorate and sodium bromate, respectively) were reinvestigated by X-ray diffraction. Contrary to previous reports, $NaCl_xBr_{1-x}O_3$ is not cubic. Data from adjacent {100} growth sectors of crystals of varying composition were refined in the triclinic space group $P1$; halate ions occupy nominally symmetry-related sites nonstatistically. Optical measurements showed that six asymmetric sectors in cubes are disposed to give an object with approximate tetrahedral point symmetry. We address forgotten anomalies, first observed almost 150 years ago, which could have been a sufficient basis for earlier structural reinvestigations. The mixed-crystal structure speaks to the general nonapplicability of the Law of Isomorphism to solid solutions. A link between optical anisotropy and nonstatistical guest site occupancy was achieved by annealing crystals between 523 and 533 K. $Na_2S_2O_3$ and $Na_2S_2O_6$ were used as habit-modifying impurities to produce $NaCl_xBr_{1-x}O_3$ crystals with {111} and $\{\bar{1}\bar{1}\bar{1}\}$ habits, respectivley. Diffraction data from {111} and $\{\bar{1}\bar{1}\bar{1}\}$ growth sectors were refined in the trigonal space group $R3$. In each case the pyramidal halate ion that was located on the special position was depleted in $BrO_3^-$. Conoscopic optical investigations nevertheless showed that the crystals are biaxial with a small $2V$ (10–15°), in marked contrast to the 90° angle in {100} crystals. We failed to reconcile the optical and X-ray structures by calculating the optical indicatrix with bond polarizability sum models. This led us to estimate the magnitude of other factors which contribute to the optical properties, including strain associated with dislocations which may exert its influence through combined piezoelectric and linear electro-optic effects.

### 1. Introduction

In the past 10 years several groups of scientists have shown differences in the activities of lattice sites exposed on growing crystallographic faces for impurities that are incorporated in the solid (Addadi, Berkovitch-Yellin, Weissbuch, Lahav & Leiserowitz, 1986; Vaida *et al.*, 1988; Weissbuch, Addadi, Lahav & Leiserowitz, 1991; Weissbuch, Popovitz–Biro, Lahav & Leiserowitz, 1995; Shimon *et al.*, 1993; Akizuki, Hampar & Zussman, 1979; Akizuki & Konno, 1985; Akizuki, 1987, 1989; McBride & Bertman, 1989; McBride, 1989). We adopted the naïve position that such distributions would be most easily interpreted in the simplest solid solutions that are easily prepared in the laboratory and, therefore, began detailed structural studies of isomorphous crystals of simple water-soluble isomorphous salts, including $Ba_xPb_{1-x}(NO_3)_2$ (Gopalan & Kahr, 1993), mixed alums and mixed dithionates (Crundwell, 1996), as well as $NaCl_xBr_{1-x}O_3$ (Gopalan, Peterson, Crundwell & Kahr, 1993).

In the latter halates we showed that cubes are formed as assemblages of six asymmetric growth sectors. Reduction of the cubic symmetry was achieved because each halate site in the unit cell of a single {100} growth sector ends up with a different population of $ClO_3^-$ and $BrO_3^-$ ions. This result was in qualitative agreement with the long-standing observation that cubes of $NaCl_xBr_{1-x}O_3$ are optically anisotropic. Nevertheless, two important questions remained unanswered: *What determined the occupancies that were observed from site to site and can we reconcile these X-ray structures and optical structures quantitatively?* In other words, is the site distribution of impurities a sufficient explanation of the observed anomalous double refraction?

One way to approach these questions would be to obtain corresponding X-ray and optical structures from crystals that had grown through surfaces other than {100}. In so doing, we intended to correlate bulk structure with idealized surface structure. In this work we exemplify the description of the cube crystals (**100**) and then demonstrate how the X-ray and optical structures change upon modifying the habit of the crystals to tetrahedra (**111** and $\bar{1}\bar{1}\bar{1}$) such that faces normal to the body diagonals of the idealized unit cell become the growing surfaces. Finally, we attempt to correlate quantitatively the measured optical indicatrix with the fine structures of the **100**, **111** and $\bar{1}\bar{1}\bar{1}$ $NaCl_xBr_{1-x}O_3$ mixed crystals.

Here, notations **100**, **111** and $\bar{1}\bar{1}\bar{1}$ refer to the general group of mixed-halate crystals with corresponding faces of principal morphological importance.

Interest in mechanisms of $NaClO_3$ crystal growth has peaked following the recent reinvestigations of the mechanism of chiral induction in stirred solutions of $NaClO_3$ (Kondepudi, Bullock, Digits & Yarborough, 1995; Kondepudi, Bullock, Digits, Hall & Miller, 1992; Kondepudi, Kaufman & Singh, 1990; McBride & Carter, 1991). That work, and the present paper, demonstrate that simple, long-standing observations of ordinary salt crystals can still pose serious challenges to contemporary crystal chemists.

## 2. Historical

### 2.1. *Optical anomalies*

Optical anisotropy in cubes of $NaClO_3$ was first observed by Mitscherlich in 1846. His work was reported to the French Academy of Sciences by Biot (1846), a pioneer in crystal optics. Biot (1842) constructed the now defunct theory of *lamellar polarization* to account for the anomalous optical anisotropy in crystals with cubic morphologies. Improved analyses led to the subsequent conclusion that the anomalous optical properties were a consequence of the presence of $BrO_3^-$. The optical anisotropy in mixed crystals of $NaCl_xBr_{1-x}O_3$ was commented on subsequently by Marbach (1854, 1855), Mallard (1884) and Wyrouboff (1890), who adopted the explanation of lamellar polarization or variants thereof. Brauns (1891), in reviewing the phenomena of anomalous birefringence, said that crystals of 100 are optically 'so complicated, that they do not provide a clear picture'.

Brauns (1898) later returned to the problem of anomalous birefringence of **100**. He made detailed observations of the optical properties of the crystals by examining thin sections of the cubes. He presented several conclusions: individual growth sectors are biaxial with an angle between optic axes ($2V$) approaching 90°; when viewed through a principal face {100}, the extinction directions bisect the crystal axes.

Despite the fact that mixed crystals 100 have served as the prototypical ideal mixed crystals for a variety of physical studies, Brauns' work was systematically overlooked. His paper suffered the fate of many other late 19th century studies of crystal optics; it was overshadowed by the revelations of X-ray diffraction studies (Kahr & McBride, 1992).

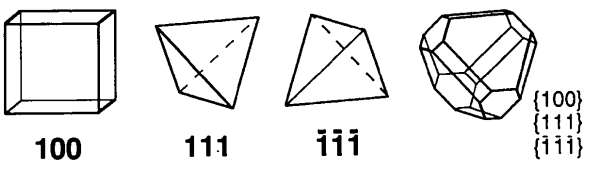


Fig. 1. Idealized morphologies of cubic mixed crystals of $NaCl_xBr_{1-x}O_3$. Left: cubes **100**; center: tetrahedra **111**; right: distorted cuboctahedron showing {$\bar{1}\bar{1}\bar{1}$} as well as {100} and {111} faces.

Recent observers treated the birefringence in the mixed crystals as a nuisance; isotropy, after all, can be achieved by annealing (Chandrasekhar & Madhava, 1969; Niedermaier & Schlenk, 1972; Chandrasekaran & Mohanlal, 1976; Sivaramakrishnan & Arunkumar, 1976; Somashekar, Prahllad & Madhava, 1987). Many of these researchers were interested in the optical rotatory power of mixed crystals, a quantity which is most easily measured in an isotropic medium (Ramachandran & Ramaseshan, 1952; Jerrard, 1954).

### 2.2. *Law of isomorphism*

Mitscherlich (1818, 1821*a*,*b*) was also responsible for the Law of Isomorphism, formulated by him as a result of his studies of crystalline transition metal sulfates and arsenates. He often noticed that when different salts contained the same amounts of water their forms were similar and that the habits of corresponding mixed crystals of these isomorphous salts often remained unchanged. Ions were exchanged willy-nilly in solid solutions without seemingly affecting structure. Our intuition about solid solutions is inherited from Mitscherlich: the solute should be distributed randomly, leaving the symmetry of the mixed crystal unperturbed from that of the end members (Kitaigorodsky, 1984).

In the mid-1980's chemists at the Weizmann Institute (Addadi *et al.*, 1986; Vaida *et al.*, 1988; Weissbuch *et al.*, 1991; Weissbuch *et al.*, 1995) studying molecular crystals and mineralogists at Tohoku University (Akizuki *et al.*, 1979; Akizuki & Konno, 1985; Akizuki, 1987, 1989) studying silicates challenged this intuition. Their work was predicated on the fact that growth-active surfaces present only a subgroup of a crystal's symmetry, therefore, solid solutions grown under kinetic control should express a reduced symmetry. In designing symmetry reduction experiments *a priori* we chose mixtures of simple isomorphous salts that formed the basis of the equivalence principle of Mitscherlich.

## 3. Experimental

### 3.1. *Optical measurements*

Optical properties of mixed crystals were studied with an Olympus BH-2 polarizing microscope in orthoscopic and conoscopic illumination. Thin sections were required for conoscopy. Epoxy slugs were cut using a diamond saw and polished to a known thickness. The thin sections were protected with a cover glass. Indices of refraction were measured by the oil immersion method and with the aid of a detent spindle stage. Refractive index oils were calibrated with an Abbe refractometer. The crystal fragment was mounted on a

glass fiber perpendicular to one of the growth faces. The retardation of mixed crystals was measured from thin sections using an Olympus Berek compensator.

### 3.2. *X-ray diffraction*

X-ray intensities were measured at room temperature on an Enraf–Nonius CAD-4 diffractometer by applying Mo $K\alpha$ radiation ($\lambda = 0.71073$ Å, graphite monochromated) and an $\omega$–$2\theta$ scan technique. The structures were refined using techniques employed in the *MolEN* package of programs (Enraf–Nonius, 1990). Empirical absorption corrections [*CAMEL* (Flack, 1977)] were applied. Atomic scattering factors and anomalous dispersion terms $f$, $\Delta f'$ and $\Delta f''$ were taken from *International Tables for X-ray Crystallography* (Cromer & Waber, 1974).

### 3.3. *Computations*

All computer programs were written in *Mathematica* 2.1. Calculations were performed on MacIntosh II Fx and Sparc workstations.

## 4. Results

### 4.1. *Crystal growth and habit modification*

We reproduced birefringent $NaCl_xBr_{1-x}O_3$ crystals by evaporating water solutions of varying composition at room temperature. More carefully controlled growths were carried out in thermostatted water baths held at 298, 308 and $318 \pm 0.1$ K. Crystals were selected from large solvent reservoirs to enforce compositional homogeneity since $NaBrO_3$ is less soluble in water (275 g $l^{-1}$) than $NaClO_3$ [790 g $l^{-1}$ (Lide, 1990)]. Pure $NaClO_3$ crystals grown in this manner are cubes displaying only {100} faces, while pure $NaBrO_3$ grow as tetrahedra {111}. Only mixed crystals containing greater than 90% $BrO_3^-$ grow as tetrahedra at room temperature, otherwise {100} faces predominate.

Von Hauer (1877) first showed that $NaClO_3$ crystallizes from water solutions with {111} faces larger than {100} faces if $SO_4^{2-}$ or $ClO_4^-$ ions are added to the solutions. Buckley (1930) expanded upon this work by establishing that $S_2O_6^{2-}$, $B_4O_7^{2-}$, $S_2O_3^{2-}$, $Cr_2O_7^{2-}$ and $CrO_4^{2-}$ ions are effective habit modifiers (Surender & Kishan Rao, 1993). These impurities were not necessarily effective at modifying the habits of the mixed crystals **100** (Bernstein, 1993). For example, $NaClO_4$ and $Na_2CrO_4$ were considerably less effective habit modifiers when the cube crystals contained substantial amounts of $BrO_3^-$. We found that $Na_2S_2O_3$ was the best habit modifier for the mixed halate crystals; when present as 5–15 mol % of the solute it gave crystals with {111} faces exclusively.

The body diagonals of $NaClO_3$ and $NaBrO_3$ crystals in the space group $P2_13$ are polar. Therefore, the $\{\bar{1}\bar{1}\bar{1}\}$ faces are distinct from the {111} faces. Slowly grown $NaBrO_3$ crystals sometimes showed developed flat $\{\bar{1}\bar{1}\bar{1}\}$ faces (Fig. 1). We were unable to epitaxially grow the mixed crystals on these surfaces in a $BrO_3^-$-rich solution containing up to 20% $ClO_3^-$. Following Buckley, Sherwood and coworkers (Sherwood, Ristic & Shevunov, 1994; Sherwood, Ristic & Wojciechowski, 1993) used $S_2O_6^{2-}$ as a habit modifier. However, the contemporary researchers came to the startling conclusion that they had produced $\{\bar{1}\bar{1}\bar{1}\}$ faces on pure $NaClO_3$ when grown from saturated solutions containing dithionate. Unlike flat, even textured {111} faces, the $\{\bar{1}\bar{1}\bar{1}\}$ faces on the $NaClO_3$ tetrahedra were rounded with roughened features. By adding 10–15 mol % of $Na_2S_2O_6$ into the crystallizing dishes, we have been able to apply this methodology to obtain mixed crystals with these well defined yet curved $\{\bar{1}\bar{1}\bar{1}\}$ faces.

### 4.2. *Chemical analysis*

Mixed halates were not conducive to electron microprobe analysis because of explosive decomposition when exposed to the electron beam. Composition was determined in **100** and **111** by analyzing for $BrO_3^-$. Samples were titrated against standard $S_2O_3^{2-}$ solutions (Swenson & Ricci, 1939). Compositional homogeneity on a large scale was confirmed by titrating dissolved fragments cut with a razor blade from the interior and exterior of single crystals. The tetrahedra enriched $BrO_3^-$ more effectively than the cubes. This observation is certainly consistent with the {111} habit of pure $NaBrO_3$.

### 4.3. *Optical structures*

4.3.1. *Cubes.* Striking demarcations in the interference colors of crystals viewed in crossed polarized light revealed six growth sectors tiled in such a way that they mimicked a cubic form {100}. In order to clearly observe the optical properties of individual growth sectors we prepared polished thin sections. Epoxy slugs containing single crystals were mounted on ground glass slides. The slugs were cut with a diamond saw and polished. Thickness was measured with microcalipers and varied between 71 and 96 μm.

When polarized light is incident to a growth face the relative retardation is maximized and the vibration directions are oriented diagonally in the square face. Of the crystal's many optical characteristics, this aspect is the simplest to detect microscopically and it is inviolable; neither composition nor growth conditions of **100** cause a deviation of the vibration directions from the diagonal positions. Viewed in an orthogonal direction, the vibrations are aligned with cube edges.

By viewing several thin sections from individual crystals, as did Brauns (1898), we constructed the relationships among the optical indicatrices (Shubnikov, 1960; Hartshorne & Stuart, 1970) in each growth sector. Adjacent {100} sectors are typically related to one another optically by threefold rotations about the body

diagonals to give an assembly that optically appears to have $T$ (23) point symmetry. Less regular arrangements are sometimes observed. Fig. 2 shows the vibration directions in a cube that has been projected in two dimensions such that we may view the six faces with respect to one another, and it confirms Brauns' (1898) earlier result.

Optical constants for single sectors mounted with epoxy on a detent spindle stage (Bloss, 1981) were measured by the oil immersion method. For single growth sectors excised from crystals with varying composition we always measured $n_\alpha$ and $n_\gamma$ to be in the plane of the growth face (Gopalan *et al.*, 1993). The calculated biaxial angle ($2V$) was between 65 and 90° for various fragments. Conoscopic interference figures confirmed that $2V$ was close to 90°.

More reliable optical constants were obtained by measuring the relative retardation of polarized light in the polished thin sections (Fig. 3) with a Berek Compensator. The birefringence of {100} sectors viewed normal to the growth face tended to decrease with increasing $BrO_3^-$ concentration in the mixed crystals (Fig. 4).

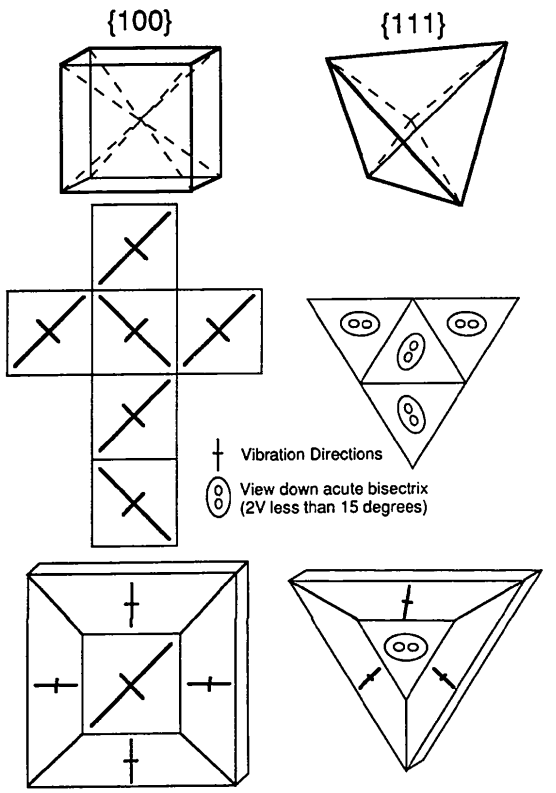


Fig. 2. Optical tilings. Top: {100} and {111} growth sectors of $NaCl_xBr_{1-x}O_3$ in **100** and **111**, respectively; center: expanded view of cube and tetrahedron as seen normal to each face (vibration directions and optic axes are marked); bottom: cube and tetrahedron in thin section.

4.3.2. *Tetrahedra.* Crystals of the form **111** and $\bar{1}\bar{1}\bar{1}$ are also birefringent. Thin slices parallel to any {111} face show optically discrete growth sectors. However, the optical properties are quite distinct from the {100} crystals. The inclination between the optic axes ($2V$) as evidenced by conoscopy is now 10–15° compared with 90° in cubic crystals with comparable composition. That is, optically, the crystals are nearly uniaxial with the acute bisectrix normal to the {111} face. A nearly uniaxial crystal would be in accord with the local symmetry argument since the {111} faces have trigonal symmetry. In triangular thin sections cut parallel to {111} faces, the vibration directions in the three perimeter sectors were not exactly parallel and perpendicular to the sides of the triangle, but were misoriented by ~5°.

As can be seen from Fig. 4, the birefringence of {111} polished thin sections tended to have the opposite behavior from the {100} crystals; it increased with increasing $BrO_3^-$ concentration over the range of solution compositions 10–90%. The optical properties of the $\bar{1}\bar{1}\bar{1}$ crystals were similar to the **111** crystals.

### 4.4. *X-ray structures*

4.4.1. *Cubes.* We polished the bottom (surface resting upon the crystallizing dish) and top of crystals with a regular cubic habit by abrasion against sintered glass plates. Side sectors showing homogeneous interference colors in crossed polarized light were chosen for further investigation. Cube fragments (~0.05 $mm^3$) were excised with a razor blade and mounted in a known orientation for X-ray diffraction studies. The entire operation was performed on the microscope stage, enabling us to mount the growth face perpendicularly to the glass fiber used in our diffraction experiments. In this way we were able to establish the Miller indices of the growth face for all fragments reported in this work with *CAD*-4 subroutines.

Prior to our communication (Gopalan *et al.*, 1993) the only other single crystal diffraction study of the mixed system $NaCl_xBr_{1-x}O_3$ had been undertaken by Raja, Mohanlal & Chandrasekaran (1984). Their results were based on the structure determination for one composition, $NaCl_{0.7}Br_{0.3}O_3$. They reported statistical guest occupancies and a cubic $P2_13$ structure, despite the fact that this cubic structure is incompatible with the known optical characteristics.

We studied mixed crystals with a variety of compositions, as seen in structures (I)–(XIII) in Table 1. All fragments have monoclinic lattice parameters in that the measured $\beta$'s were between 90.08 (2) and 90.22 (2)°. A standard ammonium tartrate crystal was used periodically to check the diffractometer alignment, thereby confirming that these deviations from 90° were indeed significant. We also found no evidence in precession photographs for superstructures, nor did Raja *et al.* (1984). $\beta$ does not vary systematically with composition for crystals containing between 30 and 80% $BrO_3^-$.

Based on the structure of the pure halates ($P2_13$) and the local symmetry argument one would expect a monoclinic structure since the only symmetry operation perpendicular to a growing face is the $2_1$ axis. This appears consistent with the measured lattice constants. Since anion positions would refine as pairs with unequal $ClO_3^-$ occupancies in $P2_1$, we would expect that the $2_1$ axis relating the pairs is parallel to *b*. Upon indexing the faces of the oriented fragments, we found that the growth faces corresponded to (100) or (001). This would imply that the $2_1$ axis *lies in the plane* of the growth face, not perpendicular to it.

A monoclinic indicatrix would require that one of the principal axes coincide with [010] and that the two other principal elements lie in the (010) plane. Minimum and maximum experimentally measured directions lie in the growth plane containing *b*, which is apparently inconsistent with the optical requirements. In the absence of other effects, the optical and crystallographic observations may be reconciled if the sectors are all triclinic,

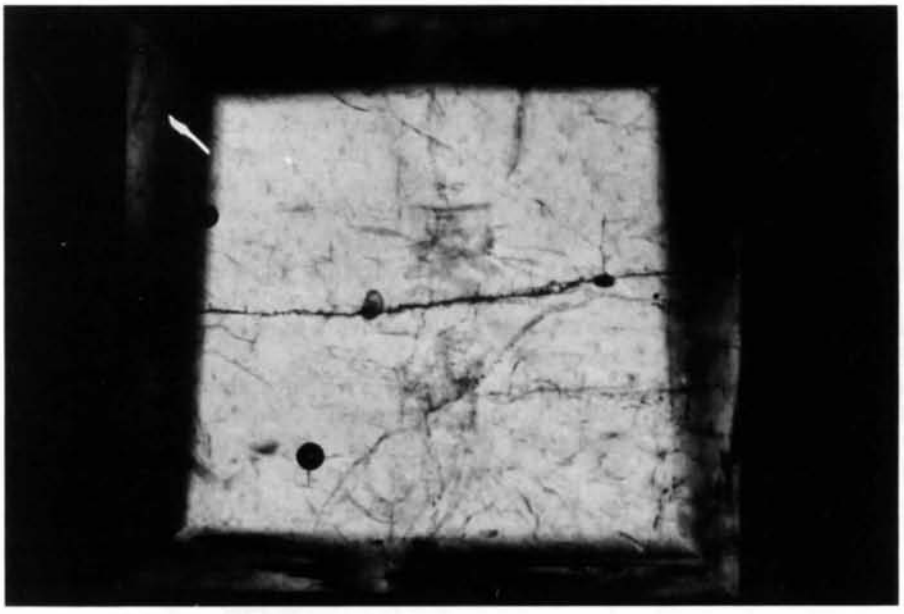

(*a*)

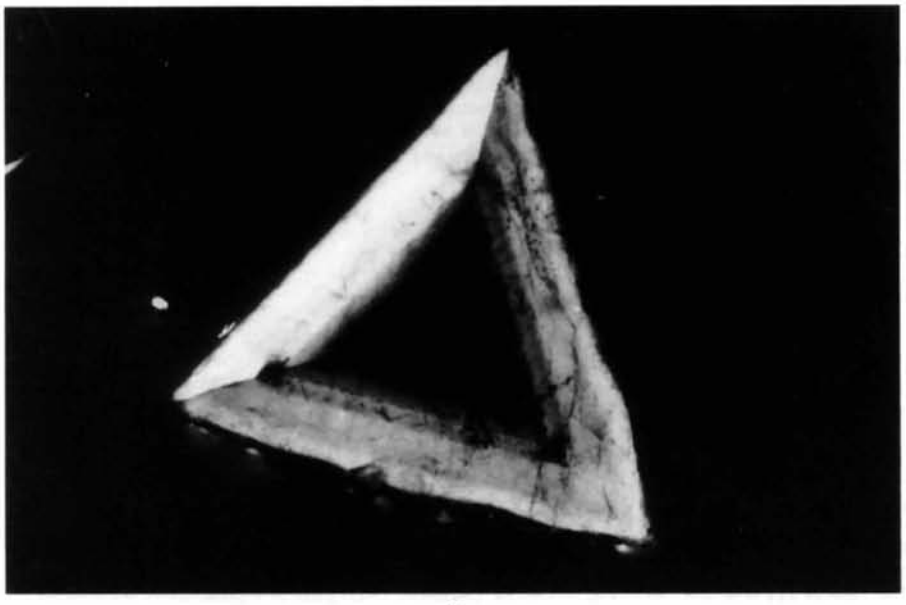

(*b*)

Fig. 3. Photomicrographs of thin sections (μm) viewed in crossed polarized light. (*a*) **100** (×40) with composition $NaCl_{0.4}Br_{0.6}O_3$. Circular features are air bubbles trapped in epoxy. (*b*) **111** (×60) with compostion $NaCl_{0.2}Br_{0.8}O_3$.

thereby lifting the symmetry restrictions on the optical indicatrix.

Crystallographic refinements for all the fragments were carried out in $P1$. Refinement strategies for the data in (I)–(V) were discussed in an earlier communication (Gopalan *et al.*, 1993). Refinements were carried out using constrained idealized as well as averaged halate geometries. These alternative models had indistinguishable effects on the fitted site occupancies. Crystal handedness was determined by comparative refinements of enantiomorphous structures and by comparing those reflections most sensitive to anomalous dispersion with values calculated for the two enantiomorphs. Enantiomorph designations were assigned and refer to the handedness of the mixed crystal to the dextrorotatroy or levorotatory form of $NaClO_3$, as given by Ramachandran & Chandresekaran (1957). For $P1$ refinements of (VII) and (VIII), where the four halate sites in the unit cell are not linked by symmetry, the $ClO_3^-$ occupancies amounted to 0.60 (1), 0.80 (1), 0.56 (1), 0.76 (1) and 0.36 (1), 0.54 (1), 0.36 (1), 0.60 (1), respectively. These positions correspond to Wyckoff (*a*) in $P2_13$ for a crystal grown through the (001) face.

To establish the validity of the $P1$ refinements, comparisons were undertaken in $P12_11$ and $P2_13$ (Table 1). Refinements diverged in $P2_11$ and $P112_1$. For example, in (II): $P2_13$ ($R = 0.064$, $wR = 0.118$, $R_m = 0.069$); $P12_11$ ($R = 0.031$, $wR = 0.042$); $P1$ ($R = 0.029$, $wR = 0.037$). Here, $R = \Sigma|F_o - F_c|/\Sigma F_o$, $wR = [\Sigma w|F_o - F_c|^2/\Sigma|F_o|^2]^{1/2}$, where $w = 1/\sigma|F_o|^2$, $R_m = \Sigma|F_{av}^2 - F_i^2|/\Sigma|F_i|^2$, where $F_{av}$ is the average of the set of observed symmetry-related structure factors and $F_i$ is the $i$th individual observed structure factor for that set. Similarly, for fragment (VII): $P2_13$ ($R = 0.055$, $wR = 0.108$, $R_m = 0.138$); $P12_11$ ($R = 0.037$, $wR = 0.060$, $R_m = 0.057$); $P1$ ($R = 0.023$, $wR = 0.035$). Lastly, in (VIII): $P2_13$ ($R = 0.090$, $wR = 0.121$, $R_m = 0.217$); $P12_11$ ($R = 0.046$, $wR = 0.058$, $R_m = 0.203$); $P1$ ($R = 0.039$, $wR = 0.048$). Application of Hamilton's (1965) test for comparative refinements invariably favors $P1$ over both $P12_11$ and $P2_13$. The rather significant violations [$I/\sigma(I) > 10$] that are observed for odd reflections of the type ($h00$), ($0k0$) and ($00l$) further substantiate the applicability of $P1$ as the best-fit model. Crystallographic data and refinement results [(I)–(XIII)] for crystal fragments containing between 19 and 91% $ClO_3^-$ are presented in the supplementary material.* A typical *ORTEP* (Johnson, 1965) representation is shown in Fig. 5.

To ensure that absorption did not bias the observed guest site selectivity, the crystal fragment (X) was ground to a sphere using a compressed air grinder following its initial data collection and refinement. A second data set was then collected and refined. The $P1$ $ClO_3^-$ site occupancies for the fragment before (X) and after (XI) grinding were 0.12 (1), 0.41 (1), 0.22 (1), 0.41 (1) and 0.14 (1), 0.39 (1), 0.21 (1), 0.40 (1), respectively. This excellent agreement suggests that absorption corrections were well applied and that they do not play a substantive artifactual role in the refined occupancies.

4.4.2. *Tetrahedra.* We have also performed extensive diffraction work on **111** crystals containing between 2 and 90% $ClO_3^-$ and a $\bar{1}\bar{1}\bar{1}$ crystal (Table 2). Following the local symmetry argument invoked earlier in the discussion for 100, we should now expect a rhombohedral structure since the only symmetry element ideally expressed by a {111} growing face is a threefold axis. In such a situation, the four anion positions that would be symmetry related in pure $NaClO_3$ refine now as two classes: one site on the threefold axis has a unique guest population, while the three other sites exhibit equal guest populations.

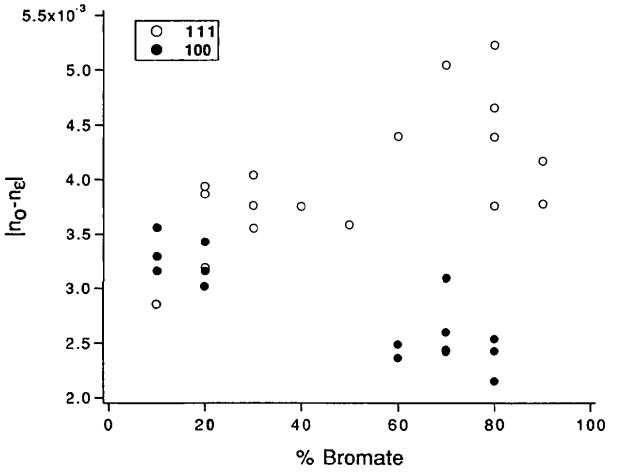


Fig. 4. Birefringence in polished thin sections as a function of $BrO_3^-$ concentration. The view in **100** is normal to the growth face, which is along the [100] for a (100) sector. The view in **111** is at 109° to the growth face normal, which is [111] for a (111) sector.

* Lists of atomic coordinates, anisotropic displacement parameters and structure factors have been deposited with the IUCr (Reference: BK0040). Copies may be obtained through The Managing Editor, International Union of Crystallography, 5 Abbey Square, Chester CH1 2HU, England.

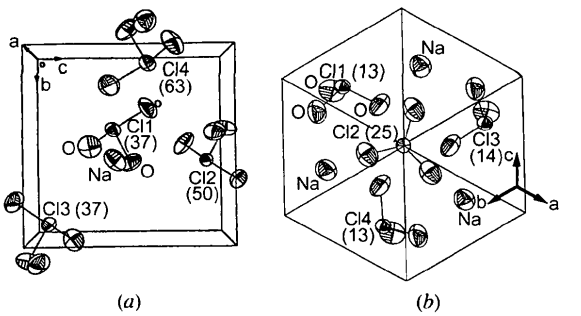


Fig. 5. *ORTEP* (Johnson, 1965) plots of representative refinements for crystals (*a*) **100** and (*b*) **111**.

Table 1. *Crystallographic data and selected refinement parameters for single* **100** *growth sectors of* $NaCl_xBr_{1-x}O_3$

| | (I) | (II) | (III) | (IV) | (V) | (VI) | (VII) | (VIII) | (IX) | (X) | (XI) | (XII) | (XIII) |
|---|---|---|---|---|---|---|---|---|---|---|---|---|---|
| % Cl | 48 | 47 | 77 | 36 | 20 | 48 | 67 | 47 | 19 | 29 | 29 | 19 | 18 |
| (*hkl*) growth face | (001) | (001) | (100) | (100) | (001) | (001) | (001) | (001) | (001) | (001) | (001) | (001) | (001) |
| Space group | *P*1 | *P*1 | *P*1 | *P*1 | *P*1 | $P2_13$ | *P*1 | *P*1 | *P*1 | *P*1 | *P*1 | *P*1 | $P2_13$ |
| *a* (Å) | 6.636 (2) | 6.630 (2) | 6.600 (1) | 6.666 (1) | 6.683 (1) | 6.648 (1) | 6.627 (1) | 6.652 (1) | 6.689 (1) | 6.6726 (8) | 6.673 (1) | 6.6825 (6) | 6.6840 (9) |
| *b* (Å) | 6.638 (1) | 6.635 (1) | 6.610 (2) | 6.668 (1) | 6.682 (1) | | 6.625 (1) | 6.647 (1) | 6.690 (1) | 6.674 (1) | 6.6707 (9) | 6.686 (1) | |
| *c* (Å) | 6.642 (1) | 6.635 (1) | 6.605 (2) | 6.669 (1) | 6.683 (1) | | 6.630 (1) | 6.654 (1) | 6.688 (1) | 6.671 (1) | 6.6707 (6) | 6.6825 (7) | |
| $\alpha$ (°) | 89.97 (1) | 89.96 (2) | 90.01 (2) | 89.99 (1) | 89.97 (1) | | 90.01 (1) | 90.04 (1) | 90.01 (1) | 90.00 (1) | 90.00 (1) | 90.04 (1) | |
| $\beta$ (°) | 90.18 (2) | 90.21 (2) | 90.08 (2) | 90.18 (1) | 90.17 (1) | | 90.19 (2) | 90.19 (2) | 90.15 (1) | 90.22 (1) | 90.22 (1) | 90.17 (1) | |
| $\gamma$ (°) | 90.02 (1) | 90.04 (2) | 90.02 (2) | 90.05 (2) | 90.04 (1) | | 89.99 (1) | 89.99 (1) | 89.99 (1) | 89.99 (1) | 90.00 (1) | 89.96 (1) | |
| $R(F_o)$ | 0.041 | 0.029 | 0.039 | 0.049 | 0.029 | 0.022 | 0.023 | 0.039 | 0.041 | 0.034 | 0.033 | 0.048 | 0.030 |
| $wR(F_o)$ | 0.067 | 0.037 | 0.052 | 0.073 | 0.038 | 0.033 | 0.035 | 0.048 | 0.056 | 0.045 | 0.043 | 0.055 | 0.038 |
| $R_m(P2_13)$ | 0.105 | 0.069 | 0.097 | 0.131 | 0.076 | | 0.138 | 0.217 | 0.179 | 0.048 | 0.059 | 0.070 | |
| $R_m(P2_1)$ | | | 0.054 | 0.076 | 0.053 | | 0.057 | 0.203 | 0.044 | 0.033 | 0.029 | 0.051 | |
| $P_{Cl(1)}$ | 0.36 (1) | 0.37 (1) | 0.70 (1) | 0.29 (1) | 0.11 (1) | 0.48 (1) | 0.60 (1) | 0.36 (1) | 0.12 (1) | 0.12 (1) | 0.14 (1) | 0.10 (1) | 0.18 (1) |
| $P_{Cl(2)}$ | 0.53 (1) | 0.50 (1) | 0.87 (1) | 0.41 (1) | 0.25 (1) | | 0.80 (1) | 0.54 (1) | 0.25 (1) | 0.41 (1) | 0.39 (1) | 0.19 (1) | |
| $P_{Cl(3)}$ | 0.41 (1) | 0.37 (1) | 0.74 (1) | 0.31 (1) | 0.10 (1) | | 0.56 (1) | 0.36 (1) | 0.12 (1) | 0.22 (1) | 0.21 (1) | 0.10 (1) | |
| $P_{Cl(4)}$ | 0.64 (1) | 0.63 (1) | 0.79 (1) | 0.39 (1) | 0.36 (1) | | 0.76 (1) | 0.60 (1) | 0.30 (1) | 0.41 (1) | 0.40 (1) | 0.35 (1) | |

Table 2. *Crystallographic data and selected refinement parameters for single* **111** *growth sectors [(I)–(VIa)] and a single* $\bar{1}\bar{1}\bar{1}$ *growth sector [(VII)–(VIIa)] of* $NaCl_xBr_{1-x}O_3$

| | (I) | (II) | (II*a*) | (III) | (IV) | (IV*a*) | (V) | (V*a*) | (VI) | (VI*a*) | (VII) | (VII*a*) |
|---|---|---|---|---|---|---|---|---|---|---|---|---|
| % Cl | 18 | 2 | 2 | 3 | 16 | 16 | 36 | 35 | 90 | 88 | 7 | 6 |
| (*hkl*) growth face | ($\bar{1}\bar{1}$1) | (111) | (111) | ($\bar{1}\bar{1}$1) | ($\bar{1}\bar{1}$1) | ($\bar{1}\bar{1}$1) | ($\bar{1}\bar{1}$1) | ($\bar{1}\bar{1}$1) | ($\bar{1}\bar{1}$1) | ($\bar{1}\bar{1}$1) | ($\bar{1}\bar{1}\bar{1}$) | ($\bar{1}\bar{1}\bar{1}$) |
| Space group | *P*1 | *P*1 | *R*3 | *P*1 | *P*1 | *R*3 | *P*1 | *R*3 | *P*1 | *R*3 | *P*1 | *R*3 |
| *a* (Å) | 6.6997 (7) | 6.7024 (5) | 6.697 (1) | 6.7045 (7) | 6.7018 (7) | 6.692 (1) | 6.664 (1) | 6.666 (1) | 6.598 (1) | 6.598 (1) | 6.6896 (7) | 6.685 (1) |
| *b* (Å) | 6.7003 (5) | 6.7039 (5) | | 6.7049 (5) | 6.7018 (6) | | 6.667 (1) | | 6.593 (1) | | 6.6867 (7) | |
| *c* (Å) | 6.6998 (6) | 6.7031 (5) | | 6.7024 (6) | 6.7013 (5) | | 6.667 (1) | | 6.593 (1) | | 6.6790 (7) | |
| $\alpha$ (°) | 90.08 (1) | 90.13 (1) | 90.00 (1) | 90.06 (1) | 90.08 (1) | 90.00 (1) | 90.16 (2) | 90.00 (1) | 90.00 (1) | 90.00 (1) | 89.94 (1) | 90.00 (1) |
| $\beta$ (°) | 90.12 (1) | 90.14 (1) | | 90.04 (1) | 90.11 (1) | | 90.12 (1) | | 90.02 (1) | | 89.84 (1) | |
| $\gamma$ (°) | 89.94 (1) | 89.89 (1) | | 89.95 (1) | 89.92 (1) | | 89.88 (1) | | 90.01 (1) | | 89.76 (1) | |
| $R(F_o)$ | 0.034 | 0.031 | 0.029 | 0.035 | 0.031 | 0.035 | 0.046 | 0.063 | 0.029 | 0.028 | 0.049 | 0.033 |
| $wR(F_o)$ | 0.044 | 0.044 | 0.040 | 0.047 | 0.042 | 0.045 | 0.055 | 0.076 | 0.043 | 0.033 | 0.059 | 0.040 |
| $R_m(P2_13)$ | 0.116 | 0.094 | 0.094 | 0.090 | 0.170 | 0.170 | 0.403 | 0.403 | 0.073 | 0.073 | 0.036 | 0.036 |
| $R_m(R3)$ | 0.092 | 0.088 | 0.088 | 0.077 | 0.067 | 0.067 | 0.246 | 0.246 | 0.068 | 0.068 | 0.501 | 0.501 |
| $P_{Cl(1)}$ | 0.16 (1) | 0.06 (1) | 0.06 (1) | 0.01 (1) | 0.14 (1) | 0.22 (1) | 0.30 (1) | 0.52 (1) | 0.90 (1) | 0.91 (1) | 0.11 (2) | 0.11 (2) |
| $P_{Cl(2)}$ | 0.28 (1) | 0.00 (1) | 0.01 (1) | 0.13 (1) | 0.25 (1) | 0.11 (1) | 0.52 (1) | 0.30 (1) | 0.93 (1) | 0.87 (1) | 0.06 (2) | 0.04 (2) |
| $P_{Cl(3)}$ | 0.15 (1) | 0.00 (1) | | 0.01 (1) | 0.13 (1) | | 0.33 (1) | | 0.89 (1) | | 0.05 (2) | |
| $P_{Cl(4)}$ | 0.15 (1) | 0.00 (1) | | 0.01 (1) | 0.14 (1) | | 0.30 (1) | | 0.89 (1) | | 0.06 (2) | |

Comparative refinements favor *R*3 over $P2_13$ and *P*1 within the constraints imposed by Hamilton's test. For example, in structure (II) (Table 2): $P2_13$ ($R = 0.029$, $wR = 0.056$, $R_m = 0.094$); *R*3 ($R = 0.029$, $wR = 0.050$, $R_m = 0.088$); *P*1 ($R = 0.031$, $wR = 0.044$). Structure (II) contains only 2% $ClO_3^-$ and the crystals are not expected to show any remarkable site selectivity. We repeated a similar analysis for structure (V) containing 36% $ClO_3^-$: $P2_13$ ($R = 0.061$, $wR = 0.078$, $R_m = 0.403$); *R*3 ($R = 0.063$, $wR = 0.076$, $R_m = 0.131$); *P*1 ($R = 0.046$, $wR = 0.055$). The refinements in the $P2_13$ model could not be extended to the anisotropic stage. For *P*1 refinements of (V), the $ClO_3^-$ occupancies for the four sites were 0.30 (1), 0.52 (1), 0.33 (1) and 0.30 (1). Six **111** structures are presented in the supplementary material [(I)–(VI*a*)], as well as one $\bar{1}\bar{1}\bar{1}$ structure [(VII)–(VII*a*)].

Upon indexing the faces of the {111} and {$\bar{1}\bar{1}\bar{1}$} fragments, we were able to establish that the X-ray crystallographic threefold axis is perpendicular to the plane of the growth face. This situation contrasts with our observations for the crystals of the {100} habit, where the $2_1$ axis lies in the plane of the growth face. A representative *ORTEP* drawing is shown in Fig. 5.

### 4.5. *Annealing experiments*

4.5.1. *Cubes.* We established a relationship between optical aniostropy and nonstatistical guest site occupancies by annealing crystal (I) in a sand bath at 531 K for 4 h (Gopalan *et al.*, 1993). The formerly biaxial fragment became isotropic and $\beta$ diminished from 90.18 (2) to 90.02 (1)°. The X-ray structure now displayed a statistical distribution of $ClO_3^-$ site occupancies in *P*1, 0.48 (1), 0.50 (1), 0.48 (1) and 0.50 (1), with $R = 0.022$, $wR = 0.033$. This was the first structure [(VI)] satisfactorily refined in $P2_13$ with $R = 0.027$, $wR = 0.041$, $R_m = 0.076$. The value of $R_m$ before annealing was 0.105. A second crystal (XII) was annealed at 523 K for 4 h. As before, the crystal became isotropic with $\beta$ diminishing from 90.17 (1)° for the formerly biaxial sector to 90.00 (1)°. The refined occupancies for the

unannealed fragment (XII) in $P\bar{1}$ are 0.10 (1), 0.19 (1), 0.10 (1) and 0.35 (1), where $R = 0.048$ and $wR = 0.055$. For the annealed fragment (XIII), a similar refinement in $P\bar{1}$ results in site occupancies of 0.18 (1), 0.18 (1), 0.18 (1) and 0.18 (1). As with (V), we were able to refine (XIII) after annealing in $P2_13$ satisfactorily with $R$ = 0.030 and $wR$ = 0.038.

4.5.2. *Tetrahedra.* On heating, the biaxial cubes become isotropic smoothly and melt uniformly at higher temperatures. In contrast, both **111** and $\bar{1}\bar{1}\bar{1}$ crystals crack and sputter before melting. We were not able to anneal either **111** or $\bar{1}\bar{1}\bar{1}$ crystals and, therefore, analogous refinements were not possible. Perhaps, unobserved fluid inclusions or the presence of small amounts of the habit-modifying agent were responsible for their demise.

## 5. Discussion

### 5.1. *Correlation of surface topographies with site occupancies*

The distribution of impurities among sites in a crystal that will become symmetry related at equilibrium depends on the structure of the growing surface, which is usually less symmetric than the bulk. In pioneering studies of solid solutions of molecular crystals, scientists at the Weizmann Institute employed the organic chemist's logic to explain site occupancies in mixed crystals of aspartic acid and asparagine, as well as cinnanamide and thienylacrylamide (Vaida *et al.*, 1988). In the first case symmetry lowering was linked to the preference of aspartic acid guests to avoid surface sites that impose O(hydroxyl)···O(carbonyl) lone-pair electron repulsions. Similarly, in the second case, solute thienylacrylamide molecules avoid sites which place the S lone-pair electrons directly into the electron-rich $\pi$-face of a neighboring cinnanamide phenyl ring. Chemists at Yale University explained patterns of orientational disorder in crystals of 1,5-dichloro-2,3-dinitrobenzene in terms of preferences for like nitro–nitro and chloro–chloro contacts (Kahr & McBride, 1992). They showed similarly that disorder in deoxypentaerythritol is driven by hydrophobic methyl–methyl interactions (Carter, 1993).

According to our X-ray diffraction studies of **100**, the local twofold symmetry of the growing faces is not even preserved. Sites that have the same surface presentation (Fig. 5) end up with vastly different occupancies of $ClO_3^-$ and $BrO_3^-$. This would seem to indicate that a crystal growth model based on an ideal surface is inadequate; it ignores important surface features such as steps, kinks, *etc.* Sherwood and coworkers have shown in photomicrographs that the 100 faces of pure $NaClO_3$ grow *via* hillocks, surface features that could be implicated in a layered growth mechanism (Hooper, Roberts & Sherwood, 1983).

Moreover, the organic chemist's intuition based on functional group interactions quickly disappears when trying to explain selectivities involving small ions such as $ClO_3^-$ and $BrO_3^-$. One way to begin to correlate distributions with surface structure would be to determine how these distributions vary for different crystallographic faces of mixed crystals with a given composition. However, in **100** all the presenting faces are related by symmetry. As we described earlier, uncommon faces can be forced to appear by adding selected habit-modifying impurities in the growth solution.

On the surfaces of the **111** and $\bar{1}\bar{1}\bar{1}$ crystals (Fig. 5), the four halate sites are partitioned into two sets having different orientations: one ion sits on a special position (threefold axis perpendicular to the growing surface), while the other three sit on general positions (with respect to the ideal surface symmetry). Each example in Table 1 shows one site enriched in $ClO_3^-$ that corresponds to the special position. On the $\{111\}$ faces the special ion presents itself from the surface in a concave orientation, whereas in the $\{\bar{1}\bar{1}\bar{1}\}$ crystals the special halate site presents itself in the convex position from the surface. We can therefore conclude that the smaller $ClO_3^-$ ions can compete effectively with $BrO_3^-$ for the occupancy of the special position normal to the growth face, irrespective of its orientation along the threefold axis.

### 5.2. *Correlation of optical and X-ray structures*

If we presume that the reduced symmetry of the mixed crystals resulting from nonstatistical guest occupancies is expressed in the refined X-ray structures and the optical anisotropy, it may be possible to calculate the essential features of the indicatrix from the X-ray structure. We term that part of the deviation from optical isotropy which results from the nonstatistical guest occupancies the structural part of the birefringence. Two approaches were attempted to calculate the structural part: summing bond polarizabilites and the application of the Lorentz Local Field Method.

5.2.1. *Summing bond polarizabilities (Weber, 1988; Denbigh, 1940; Bunn & Daubeny, 1954; McBride & Vassas, 1990).* We entertained the notion that a sum of bond polarizability tensors assigned to each halate bond and weighted according to the experimental X-ray occupancies might reproduce the observed optical indicatrix, most notably, the diagonal orientation of vibration directions in the plane of each growth face. Biaxial bond polarizability tensors for Cl—O and Br—O bonds in $ClO_3^-$ and $BrO_3^-$ were obtained from the Hartree–Fock SCF calculations of Eysel, Lipponer, Oberle & Zahn (1992) or estimated, also by Eysel (1988), from Raman intensities of $ClO_3^-$ ions in solution. The 24 symmetry-related tensors were generated, weighted and summed. The isotropic atomic polarizability for sodium was added (Pohl, 1978). The final tensor was diagonalized, thereby providing, according to the Clausius–Mossotti formula

(1) (Jaffe, 1988), the principal components of the refractive index, $n$. Here, $\epsilon$ is the relative dielectric permittivity, $\alpha$ is the electronic polarizability and $\chi$ is the dielectric susceptibility

$$(\epsilon - 1)/(\epsilon + 2) = (4\pi/3)\Sigma N_j\alpha_j, \text{ where } \epsilon = 1 + 4\pi\chi = n^2. \quad (1)$$

We cannot expect to obtain accurate absolute values of the refractive index in this way since we are starting with gas or solution phase polarizabilities. We did expect that the birefringence and indicatrix orientation should be in qualitative agreement with experiment if summing bond polarizabilities is sufficient.

We found no qualitative agreement and thus conclude that the model cannot be sufficient for explaining the observed optical properties. For **100**, we predicted in each case, according to the experimental occupancies, a maximum birefringence when viewed along [010]. The experimentally observed maximum was always seen when the crystal was viewed normal to the growth face indexed as (100) or (001). Rhombohedral **111** and $\bar{1}\bar{1}\bar{1}$ structures naturally result in calculated uniaxial optical indicatrices. The observed (10–15°) biaxial angle cannot be reconciled with trigonal symmetry.

5.2.2. *Lorentz Local Field Theory (Lorentz, 1888; Kittel, 1976; Rohleder & Munn, 1992).* A more rigorous approach to the calculation of the optical properties from nonisometric crystal structures involves the application of Lorentz Local Field Theory. Lorentz suggested that the local effective field at an atom could be approximated as the sum of the dipolar fields within a cavity containing the atom in question, and a mean field outside the cavity. We adopted the implimentation of Fawcett and coworkers (2) (Bolton, Fawcett & Gurney, 1962; Fawcett, 1963). Here, $P$ is the polarization and $E$ is the total electric field at an atomic site which may be expressed as the sum of an internal field resulting from individual dipoles within a cavity and a continuum field from outside the cavity. $F_j$ is the local field at the $j$th atom and $\beta$ is the Lorentz factor

$$P = \chi E = \Sigma N_j p_j = \Sigma N_j\alpha_j F_j, \text{ where}$$
$$E = \Sigma\alpha_j F_j[(3r_i r_j - r_i^2)/r_j^5] + \beta\Sigma\alpha_j F_j. \quad (2)$$

To ensure the validity of the use of the cubic unit cell in the calculation of the refractive indices, we also used a nonspherical (elliptical) cavity (Crisp & Wamsley, 1980). Convergence of lattice sums was performed in reciprocal space (de Wette, 1961; de Wette & Schacher, 1965). The correction to the refractive indices was small ($\Delta n < 0.001$) and well within the limits of experimental error. We thus concluded that results of less elaborate computations using spherical cavities can be accepted as the structural birefringence.

Both the simple bond additivity approach and the Lorentz Local Field Method gave results that were in essential agreement with one another, but not with experiment. Again we find in each **100** case that the greatest retardation is calculated to be always along $b$ and never along $a$ or $c$, as we find experimentally (Fig. 6). The shapes of the observed and calculated tensors are comparable, $2V_{calc} \simeq 90°$, but the calculated tensors are misoriented by 90° when compared with experiment; that is, the vibration directions in the calculated optical stuctures were diagonally oriented in the $b$ face.

### 5.3. *Elastic effects on optical properties*

At this junction, we were forced to consider other physical effects that could give rise to the observed optical anisotropy in **100**, **111** and $\bar{1}\bar{1}\bar{1}$. There have been reports of birefringence induced in pure $NaClO_3$ and $NaBrO_3$ under externally applied conditions that are relevant to the development of the discussion of anomalous birefringence in the mixed crystals. First we discuss elastic effects and finally plastic effects. Since we are not applying elastic stresses to our crystals, the discussion of elastic effects is pedagogical but necessary. The optical rotation was assumed to have a small effect on the birefringence and was neglected in all calculations.

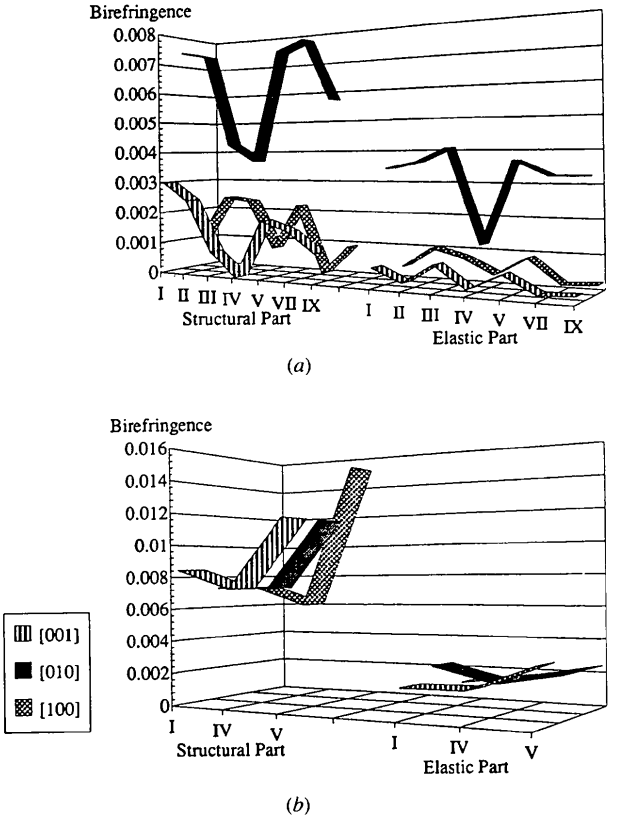


Fig. 6. Calculated structural and elastic contributions to the birefringence in (*a*) **100** and (*b*) **111**. Roman numerals refer to crystals in Tables 1 and 2. In each **100** case, the maximum relative retardation of polarized light is along [010], in stark contrast with experiment.

5.3.1. *Photoelastic effect.* Brewster (1815, 1816, 1818) first demonstrated that isotropic bodies that are placed under nonuniform stress become birefringent. This general phenomenon of photoelasticity was thoroughly reviewed by Narasimhamurty (1981). Specifically, the change in the optical indicatrix ($\Delta B_{ij}$) is related to the strain tensor ($\epsilon_{kl}$) by the fourth-rank piezo-optic tensor ($p_{ijkl}$), whose elements are constrained by the symmetry of the medium (3). The photoelastic constants ($p_{ij}$ in compact notation) have been determined (Ramachandran & Chandrasekaran, 1951)

$$\Delta B_{ij} = p_{ijkl}\epsilon_{kl}, \text{ where}$$

$$p_{ij} = \begin{vmatrix} p_{11} & p_{12} & p_{13} & 0 & 0 & 0 \\ p_{13} & p_{11} & p_{12} & 0 & 0 & 0 \\ p_{12} & p_{13} & p_{11} & 0 & 0 & 0 \\ 0 & 0 & 0 & p_{44} & 0 & 0 \\ 0 & 0 & 0 & 0 & p_{44} & 0 \\ 0 & 0 & 0 & 0 & 0 & p_{44} \end{vmatrix}. \quad (3)$$

Stress-induced birefringence in $NaClO_3$ and $NaBrO_3$ was previously reported by Brauns (1898). In **100**, **111** and $\bar{1}\bar{1}\bar{1}$ the birefringence can be affected locally by applying a pin to the surface of the crystal. Under modest pressures, these local changes are fully reversible. However, the permanent birefringence of the mixed crystals is a consequence of growth; it is not the result of applied external stress. Nevertheless, we wanted to determine the magnitudes of $\Delta B_{ij}$ that might be induced in **100**, **111** and $\bar{1}\bar{1}\bar{1}$ as a consequence of elastic deformation.

X-ray diffraction indicated that the unit cell for the mixed crystals deviated measureably from cubic dimensions. We calculated the magnitude of the birefringence that we would expect in isotropic, cubic mixed crystals of $NaClO_3$ and $NaBrO_3$ were its lattice deformed to the extent that was seen experimentally. We are presuming that the lattice deformation in the mixed crystals resulted wholly from external stress. Thus, taking the change of lattice parameters from those of an ideal cubic structure as a measure of distortion, we were able to form a strain tensor (Von W. Sterzel & Knöll, 1973).

We used a photoelastic tensor, shown as in (3), in the compact matrix notation, having the same symmetry as in pure $NaClO_3$ or $NaBrO_3$, with constants taken as the weighted average of those for the pure end members weighted according to the experimental composition (Hellwege, 1969). However, we cannot consider photoelasticity in the absence of other elastic effects such as piezoelectricity and the linear electro-optic effect that may act synergistically to alter the crystal's optical properties.

5.3.2. *Linear electro-optic effect (Pockels effect).* An applied electric field can also have significant optical consequences in $NaClO_3$ and $NaBrO_3$. The change in the optical indicatrix of a cubic crystal can be related to the direction of the applied field (4) with the third rank electro-optic tensor $r_{ijk}$ shown in compact matrix notation for class $T$ (23). Again, constants were taken as the weighted average of the end members (Hellwege, 1969)

$$\Delta B_{ij} = r_{ijk}E_k, \; r_{ij} = \begin{vmatrix} 0 & 0 & 0 \\ 0 & 0 & 0 \\ 0 & 0 & 0 \\ r_{41} & 0 & 0 \\ 0 & r_{41} & 0 \\ 0 & 0 & r_{41} \end{vmatrix}. \quad (4)$$

Pockels (1906) discovered the linear electro-optic effect and described the reorientation of the optical indicatrix in crystals of $NaClO_3$ in the presence of an applied electric field. He concluded that, 'If the lines of force are parallel to a cube normal, then the binormals are parallel to the two other cube normals and the largest path difference lies in the direction of the lines of force' (Kaminow, 1974). The biaxial angle is 90° and the principal axes of the indicatrix are aligned with one cube axis and oriented at 45° to the other two orthogonal cube axes.

Thus, **100** appear optically as if an electric field were applied in each growth sector at a right angle to the bounding face. Brauns recognized the relationship between the optical properties in single {100} sectors of **100** crystals and Pockels' observations of pure $NaClO_3$ under the application of electric fields. Brauns remarked that building impurity ions into the lattice in the mixed crystals has the same effect in the optically anomalous crystals as placing an optically normal crystal in an applied field.

5.3.3. *Piezoelectricity.* The photoelastic and linear electro-optic effects are linked in noncentrosymmetric crystals by the piezoelectric effect, a third rank tensor $d_{ijk}$ that relates the electric moment produced inside a crystal with the strain $\epsilon_{jk}$ (5). Again, the piezoelectric tensor is expressed in the compact matrix notation for class $T$ (23)

$$E_i = d_{ijk}\epsilon_{jk}, \; d_{ij} = \begin{vmatrix} 0 & 0 & 0 & d_{14} & 0 & 0 \\ 0 & 0 & 0 & 0 & d_{14} & 0 \\ 0 & 0 & 0 & 0 & 0 & d_{14} \end{vmatrix}. \quad (5)$$

In piezoelectric crystals, applied stress may produce an electric dipole moment in a crystal and thereby change the optical properties *via* a combination of the direct photoelastic and indirect electro-optic effects. Pockels (1893) was also the first to obtain the piezoelectric constant in $NaClO_3$ (Voigt, 1910). Mason (1954) provided the modern values.

Finally, we obtain the net formula for the change of the optical indicatrix *via* a combination of photoelastic, piezoelectric and linear-electrooptic effects (6)

$$\Delta B_{ij} = (r_{ijk}d_{klm} + p_{ijlm})\epsilon_{lm}. \quad (6)$$

Again, the two third rank tensors (4 and 5) are assumed to have the same symmetry as pure $NaClO_3$ and $NaBrO_3$, with constants taken as weighted averages according to the experimental composition.

If we presume that the deformed lattice affects the optical indicatrices not only *via* the photoelastic effect, but through piezooptic action as well, we calculate a new change in the optical indicatrix. We term this the *elastic* part of the birefringence. From Fig. 7 it is evident that for **100** the hypothetical elastic part of the birefringence ($<0.005$) is of the same magnitude as the structural part ($<0.008$), both of which compare reasonably with experimental magnitudes (0.004–0.0012).

### 5.4. *Plastic effects on optical properties*

In the above discussion we argue that an accurate description of anomalous birefringence must take into account structural and elastic effects, if the latter were applied. Elastic distortions are reversible; in contrast, plastic distortions (Sprackling, 1976) are those that do not disappear upon withdrawal of the external forces acting on the system. Once again, it was Brewster (1818) who first obtained optical evidence of plastic deformations in crystals, although a structural interpretation was not possible in his time. We now know that a common source of strain and its associated birefringence in crystals are dislocations (Nabarro, 1987).

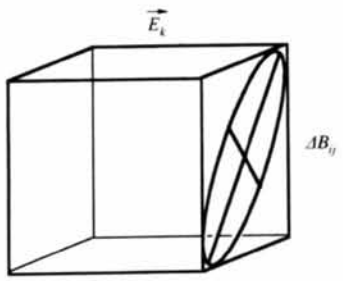


Fig. 7. Scheme showing the distortion of the isotropic indicatrix on application of an electric field $E_k$ parallel to [100].

Obreimow & Schubnikoff (1927) first showed that the slip planes in NaCl correspond to doubly refracting bands. Nye (1949) identified similar bands in rolled AgCl as the result of edge dislocations. Chou (1963) calculated the strain tensors associated with particular dislocations in simple cubic crystals. Kataoka, Okuda & Yamada (1972) showed that stress at any point in mixed KCl/KBr crystals may be evaluated by superimposing stresses from neighboring dislocations. It may be possible that a permanent stress birefringence results from dislocations in **100**, **111** and $\bar{1}\bar{1}\bar{1}$.

The contemporary literature on stress birefringence is overwhelmingly dominated by studies on crystals in isotropic classes $O_h$ ($m3m$) [*e.g.* KCl (Sakamoto & Yamada, 1980)] and $T_h$ ($m3$) [*e.g.* $Ba(NO_3)_2$ (Ge, Wang & Ming 1993)]. However, comparable studies on the noncentrosymmetric class $T$ (23) are conspicuously absent. Presumably, this is because of complications that arise in piezoelectric crystals such as $NaClO_3$ and $NaBrO_3$. In Fig. 8 we can observe birefringent bands, 0.1 mm in width, that stand out in the lateral growth sectors of a sectioned 100 crystal. These are undoubtedly evident because our view of the lateral sectors coincides with an optic axis in the material. These fine structures are absent in the central square through which we see the maximum relative retardation, normal to a growth

Fig. 8. Photomicrograph (× 200) of **100** thin section (77 μm) with composition $NaCl_{0.42}Br_{0.58}O_3$ showing optical bands, possibly due to plastic distortion. Circular features are air bubbles trapped in epoxy.

face. These bands bear a striking resemblance to the birefringent slip bands in rock salt and may be attributed to plastic deformation (Shaskol'skaya & Jui-Fang, 1960; Mendelson, 1961).

Dislocations play an important role in controlling the rate and mechanism of growth of $NaClO_3$ crystals (Mussard & Goldsztaub 1972). These dislocations have been imaged using X-ray topography (Kito & Kato, 1974; Matsunaga, Kitamura & Sungawa, 1980). In the most recent topographic study, Hooper *et al.* (1983) conclude that the predominant types of dislocation in {100} growth sectors of $NaClO_3$ are pure screw and edge dislocations of Burgers vectors, $a$<100>. Using the method of Chou (1963), we are currently trying to determine the strain fields associated with such dislocations in the sodium halates.

What remains then is the identification of the dislocations in $NaCl_xBr_{1-x}O_3$. Preliminary X-ray topographic studies of mixed $NaCl_xBr_{1-x}O_3$ crystals reveal large strains with gross misalignments of growth sectors (Vetter & Dudley, 1993). The contrast is not of sufficient resolution for inferring the nature of the dislocations that are present. However, Hussain, Subhadra & Kishan Rao (1988) have shown through etching studies that the dislocation density in $NaCl_xBr_{1-x}O_3$ rises rapidly with composition. They counted $16 \times 10^4$ cm$^{-2}$ for pure $NaClO_3$ and $121 \times 10^4$ cm$^{-2}$ in a crystal containing 30% molar fraction $BrO_3^-$.

In a review of the history of the study of anomalous birefringence in crystals Kahr & McBride (1992) outlined the important role 'stress hypotheses' played in the 19th century in organizing a wide range of aberrant optical phenomenology. Since many of the early champions of stress hypotheses referred to Brewster's discovery of photoelasticity or to geological catastrophes which may have influenced mineralogical samples, we felt that the analogy to an elastic effect clearly absent in 'as-grown' crystals was misplaced. We tended to downplay the role of stress in explaining historical optical anomalies in favor of purely structural explanations based on the selectivity of impurities at surface sites.

Our modern ideas of dislocations and plastic strains associated with them developed during the 1930's and 1940's (Hoddeson, Braun, Teichmann & Weart, 1992). Nineteenth century concepts of plastic strains in crystals were ill-defined, but it is clear the pioneering crystallographers understood that internal strains could arise in some manner from rapid cooling or precipitation. In view of our inability to provide a structural interpretation to the optical anisotropy in $NaCl_xBr_{1-x}O_3$ it is true that plastic strains and their optical manifestations amplified through piezo-optic effects may indeed be important in explaining the optical properties of a wide variety of historical optically anomalous crystals. We argue that the characterization of the type of dislocations in optically anomalous crystals is requisite for a complete understanding.

## 6. Conclusions

(1) X-ray diffraction data from birefringent growth sectors of **100** were best fit to triclinic structures ($P1$) in which $ClO_3^-$ and $BrO_3^-$ ions occupied the four lattice sites nonstatistically. The X-ray symmetry is lower than would be expected from an analysis of idealized (100) surface symmetry.

(2) X-ray diffraction data from single growth sectors of **111** and $\bar{1}\bar{1}\bar{1}$ were best fit to rhombohedral ($R3$) structures. The X-ray structures are consistent with the trigonal surface symmetry. The site on the special position is always depleted in $BrO_3^-$, irrespective of whether the halate ion is presented in a convex or concave position along the polar axis.

(3) Single growth sectors of **100** were optically biaxial with $2V = 90°$.

(4) Single growth sectors of **111** and $\bar{1}\bar{1}\bar{1}$ were also biaxial, but nearly uniaxial with $2V = 10$–$15°$.

(5) The calculated indicatrices of **100** and **111** based on the refined X-ray structures could not be reconciled in either case with the observed optical properties. These inconsistencies provide evidence of the importance of piezo-optic contributions to the observed optical properties which may result from the spontaneous strain associated with dislocations.

Thanks is offered to the Donors of The Petroleum Research Fund, administered by the American Chemical Society (ACS-PRF #24331-G6 and #27665-AC3), the Exxon Education Foundation and the National Science Foundation (CHE-9457374) for support of this research. We are grateful to Earl Geist for the preparation of thin sections, Professor Igal Szleifer for the use of his computer network and Paul Bower for access to the constant temperature baths. The present address for PG is the Materials Science Center, Indian Institute of Technology, Powai, Bombay 400 076, India.

## References

Addadi, L., Berkovitch-Yellin, Z., Weissbuch, I., Lahav, M. & Leiserowitz, L. (1986). *Top. Stereochem.* **16**, 1–85.
Akizuki, M. (1987). *Am. Mineral.* **72**, 645–648.
Akizuki, M. (1989). *Ganko*, **84**, 403–426.
Akizuki, M. & Konno, H. (1985). *N. Jahrb. Mineral. Abh.* **151**, 99–115.
Akizuki, M., Hampar, M. S. & Zussman, J. (1979). *Mineral. Mag.* **43**, 237–241.
Bernstein, J. (1993). Personal communication.
Biot, J.-B. (1842). *Mem. Acad. Sci. Inst. Fr. 2me Ser.* **18**, 539–725.
Biot, J.-B. (1846). *C. R. Seances Acad. Sci.* **23**, 909–910.
Bloss, F. D. (1981). *The Spindle Stage: Principles and Practices*, p. 40. Cambridge University Press.
Bolton, H. C., Fawcett, W. & Gurney, I. D. C. (1962). *Proc. R. Soc.* **80**, 199–208.
Brauns, R. (1891). *Die Optische Anomalien der Krystalle*, pp. 332–333. Leipzig: W. Engelmann.
Brauns, R. (1898). *N. Jahrb. Mineral. Geol. Palontol.* **1**, 40–59.

Brewster, D. (1815). *Philos. Trans. R. Soc. London*, **105**, 60–64.
Brewster, D. (1816). *Philos. Trans. R. Soc. London*, **106**, 156–178.
Brewster, D. (1818). *Trans. R. Soc. Edinburgh*, **8**, 157, 281–286, 309, 353–371.
Buckley, H. E. (1930). *Z. Krist.* **75**, 15.
Bunn, C. W. & Daubeny, R. De P. (1954). *Trans. Faraday Soc.* **50**, 1173–1177.
Carter, R. L. (1993). PhD Dissertation, Yale University.
Chandrasekaran, K. S. & Mohanlal, S. K. (1976). *Pramana*, **7**, 152–159.
Chandrasekhar, S. & Madhava, M. S. (1969). *Mat. Res. Bull.* **4**, 489–494.
Chou, Y. T. (1963). *J. Appl. Phys.* **34**, 429–433.
Crisp, G. M. & Wamsley, S.-H. (1980). *Chem. Phys. Lett.* **74**, 181–187.
Cromer, D. T. & Waber, J. T. (1974). *International Tables for X-ray Crystallography*. Birmingham: The Kynoch Press. (Present distributor Kluwer Academic Publishers, Dordrecht.)
Crundwell, G. (1996). Purdue University, PhD Dissertation.
Denbigh, K. G. (1940). *Trans. Faraday Soc.* **36**, 936–948.
Enraf–Nonius (1990). *MolEN. An Interactive Structure Solution Procedure*. Enraf–Nonius, Delft, The Netherlands.
Eysel, H. H. (1988). *Spectrochim. Acta A*, **44**, 991–997.
Eysel, H. H., Lipponer, K.-G., Oberle, C. & Zahn, I. (1992). *Spectrochim. Acta A*, **48**, 219–224.
Fawcett, W. (1963). *Proc. Phys. Soc.* **82**, 33–46.
Flack, H. D. (1977). *Acta Cryst.* A**33**, 890.
Ge, C.-Z., Wang, H.-W. & Ming, N.-B. (1993). *J. Appl. Phys.* **74**, 139–145.
Gopalan, P. & Kahr, B. (1993). *J. Solid State Chem.* **107**, 563–567.
Gopalan, P., Peterson, M., Crundwell, G. & Kahr, B. (1993). *J. Am. Chem. Soc.* **115**, 3366–3367.
Hamilton, W. C. (1965). *Acta Cryst.* **18**, 502.
Hartshorne, N. H. & Stuart, A. (1970). *Crystals and the Polarizing Microscope*. London: Edward Arnold.
Hellwege, K.-H. (1969). Editor. *Landolt–Börnstein: Numerical Data and Functional Relationships in Science and Technology: Group III. Crystal and Solid State Physics*, Vol. 2. *Elastic, Piezoelectric, Piezooptic, Electrooptic Constants and Nonlinear Dielectric Susceptibilities of Crystals*. New York: Springer-Verlag.
Hoddeson, L., Braun, E., Teichmann, J. & Weart, S. (1992). *Out of the Crystal Maze: Chapters from the History of Solid-State Physics*, Ch. 5. New York: Oxford University Press.
Hooper, R. M., Roberts, K. J. & Sherwood, J. N. (1983). *J. Mater. Sci.* **18**, 81–88.
Hussain, K. A., Subhadra, K. G. & Kishan Rao, K. (1988). *Cryst. Res. Technol.* **23**, 171–177.
Jaffe, H. W. (1988). *Crystal Chemistry and Refractivity*. New York: Cambridge.
Jerrard, H. G. (1954). *J. Opt. Soc. Am.* **44**, 634–640.
Johnson, C. K. (1965). *ORTEP*. Report ORNL-3794. Oak Ridge National Laboratory, Tennessee, USA.
Kahr, B. & McBride, J. M. (1992). *Angew. Chem. Int. Ed. Engl.* **31**, 1–26.
Kaminow, I. P. (1974). *An Introduction to Electrooptic Devices*, pp. 121–137. New York: Academic Press.
Kataoka, T., Okuda, S. & Yamada, T. (1972). *J. Appl. Phys.* **11**, 1421–1428.
Kitaigorodsky, A. I. (1984). *Mixed Crystals*, Vol. 33. *Solid-State Sciences*, p. 224. Berlin: Springer Verlag.
Kito, I. & Kato, N. (1974). *J. Cryst. Growth*, **24/25**, 544–548.
Kittel, C. (1976). *Introduction to Solid State Physics*, 5th ed., pp. 401–427. New York: John Wiley & Sons.
Kondepudi, D. K., Bullock, K. L., Digits, J. A., Hall, J. K. & Miller, J. M. (1992). *J. Am. Chem. Soc.* **115**, 10211–10216.
Kondepudi, D. K., Bullock, K. L., Digits, J. A. & Yarborough, P. D. (1995). *J. Am. Chem. Soc.* **117**, 401–404.
Kondepudi, D. K., Kaufman, R.-J. & Singh, N. (1990). *Science*, **250**, 975–976.
Lide, D. R. (1990). Editor. *CRC Handbook of Chemistry and Physics*, 71st edn. Boca Raton: CRC Press.
Lorentz, H. A. (1888). *Verhand. Akad. Wet. Amsterdam*, **26**, Collected Papers II, 71–87.
Mallard, E. (1884). *Bull. Soc. Fr. Minéral.* **7**, 349.
Marbach, H. (1854). *Ann. Phys.* **91**, 482–487.
Marbach, H. (1855). *Ann. Phys.* **94**, 412–426.
Mason, W. P. (1954). *Piezoelectric Crystals and Their Application to Ultrasonics*. New York: D. Van Nostrand.
Matsunaga, M., Kitamura, M. & Sungawa, I. (1980). *J. Cryst. Growth*, **48**, 425.
McBride, J. M. (1989). *Angew. Chem. Int. Ed. Engl.* **28**, 377–378.
McBride, J. M. & Bertman, S. B. (1989). *Angew. Chem. Int. Ed. Engl.* **28**, 330–333.
McBride, J. M. & Carter, R. L. (1991). *Angew. Chem. Int. Ed. Engl.* **30**, 293–295.
McBride, J. M. & Vassas, M. (1990). Unpublished results.
Mendelson, S. (1961). *J. Appl. Phys.* **32**, 1999–2004.
Mitscherlich, E. (1818). *Abhandlugen der Koniglichen Akademie der Wissenschaften in Berlin*, p. 427.
Mitscherlich, E. (1821*a*). *Ann. Chim.* **19**, 350–419.
Mitscherlich, E. (1821*b*). *Kungliga Akad. Handl.* 4.
Mussard, F. & Goldsztaub, S. (1972). *J. Cryst. Growth*, **13/14**, 445.
Nabarro, F. R. N. (1987). *Theory of Crystal Dislocations*. New York: Dover.
Narasimhamurty, T. S. (1981). *Photoelastic and Electro-optic Properties of Crystals*. New York: Plenum Press.
Niedermaier, T. & Schlenk, W. Jr (1972). *Chem. Ber.* **105**, 3470–3478.
Nye, J. F. (1949). *Proc. R. Soc. (London) A*, **198**, 190–204.
Obreimow, I. W. & Schubnikoff, L. W. (1927). *Z. Phys.* **41**, 907–919.
Pockels, F. (1893). *N. Jahrb. Mineral. Geol. Palontol.* **7**, 200.
Pockels, F. (1906). *Lehrbuch der Kristalloptik*, pp. 492–510. Leipzig: B. G. Teubner.
Pohl, D. (1978). *Acta Cryst.* A**34**, 574.
Raja, S. C., Mohanlal, S. K. & Chandrasekaran, K. S. (1984). *Z. Krist.* **166**, 121–127.
Ramachandran, G. N. & Chandresekaran, K. S. (1957). *Acta Cryst.* **10**, 671–675.
Ramachandran, G. N. & Chandrasekaran, V. (1951). *Proc. Ind. Acad. Sci.* **33**, 199–215.
Ramachandran, G. N. & Ramaseshan, S. (1952). *J. Opt. Soc. Am.* **42**, 49–56.
Rohleder, J. W. & Munn, R. W. (1992). *Magnetism and Optics of Molecular Crystals*. New York: John Wiley.
Sakamoto, M. & Yamada, T. (1980). *Jpn. J. Appl. Phys.* **19**, 1617–1625.
Shaskol'skaya, M. P. & Jui-Fang, S. (1960). *Sov. Phys. Crystallogr.* **4**, 74–79.

Sherwood, J. N., Ristic, R. & Shevunov, B. Yu. (1994). *J. Cryst. Growth*, **139**, 336–343.
Sherwood, J. N., Ristic, R. & Wojciechowski, K. (1993). J. *Phys. Chem.* **97**, 10774–10782.
Shimon, L. J. W., Vaida, M., Frolow, F., Lahav, M., Leiserowitz, L., Weissinger-Lewin, Y. & McMullan, R. K. (1993). *Faraday Discuss.* **95**, 307–327.
Shubnikov, A. V. (1960). *Principles of Optical Crystallography*. New York: Consultants Bureau.
Sivaramakrishnan, V. & Arunkumar, K. A. (1976). *Opt. Acta*, **23**, 209–216.
Somashekar, R., Prahllad, U. D. & Madhava, M. S. (1987). *J. Mat. Sci. Lett.* **6**, 207–208.
Sprackling, M. T. (1976). *The Plastic Deformation of Simple Ionic Crystals*. London: Academic Press.
Surender, V. & Kishan Rao, K. (1993). *Bull. Mater. Sci.* **16**, 155–158.
Swenson, T. & Ricci, J. E. (1939). *J. Am. Chem. Soc.* **61**, 1974–1977.
Vaida, M., Shimon, L. J. W., Weisinger-Lewin, Y., Frolow, F., Lahav, M., Leiserowitz, L. & McMullan, R. K. (1988). *Science (Washington)*, **241**, 1475–1479.
Vetter, W. & Dudley, M. (1993). Unpublished results.
Voigt, W. (1910). *Lehrbuch der Kristallphysik*, p. 873. Leipzig: B. G. Teubners.
Von Hauer, C. (1877). *Verh. Geol. Reichanst. Vienna*, **4**, 57–61.
Von W. Sterzel, U. & Knöll, U. (1973). *Z. Anorg. Allg. Chem.* **399**, 25–33.
Weber, H.-J. (1988). *Acta Cryst.* A**44**, 320–326.
Weissbuch, I., Addadi, L., Lahav, M. & Leiserowitz, L. (1991). *Science (Washington)*, **253**, 637–645.
Weissbuch, I., Popovitz-Biro, R., Lahav, M. & Leiserowitz, L. (1995). *Acta Cryst.* B**51**, 115–148.
Wette, F. W. de (1961). *Phys. Rev.* **123**, 103–112.
Wette, F. W. de & Schacher, G. E. (1965). *Phys. Rev. A*, **137**, 78–94.
Wyrouboff, G. (1890). *Bull. Soc. Fr. Minéral* **13**, 215–233.